DOI: 10.1002/chem.200700185

Influence of the Protonic State of an Imidazole-Containing Ligand on the Electrochemical and Photophysical Properties of a Ruthenium(II)–Polypyridine-Type Complex

Annamaria Quaranta,[a] Fabien Lachaud,[b] Christian Herrero,[a] Régis Guillot,[b] Marie-France Charlot,*[b] Winfried Leibl,*[a] and Ally Aukauloo*[a, b]

Abstract: The synthesis and characterisation of $[Ru(bpy)_2(PhenImHPh)]^{2+}$ where PhenImHPh represents the 2-(3,5-di-*tert*-butylphenyl)imidazo[4,5-*f*]-[1,10]phenanthroline ligand are described. The compounds issued from the three different protonic states of the imidazole ring $[Ru(bpy)_2(PhenImPh)]^{+}$ (**I**), $[Ru(bpy)_2(PhenImHPh)]^{2+}$ (**II**) and $[Ru(bpy)_2(PhenImH_2Ph)]^{3+}$ (**III**) were isolated and spectroscopically characterised. The X-ray structures of $[Ru(bpy)_2(PhenImPh)](PF_6)\cdot H_2O\cdot 6\,MeOH$, $[Ru(bpy)_2(PhenImHPh)](NO_3)_2\cdot H_2O\cdot 3\,MeOH$ and $[Ru(bpy)_2(PhenImH_2Ph)](PF_6)_3\cdot 5\,H_2O$ are reported. Electrochemical data obtained on these complexes indicate almost no potential shift for the $Ru^{III/II}$ redox couple. Therefore a Coulombic effect between the imidazole ring and the metal centre can be ruled out. The monooxidised forms of **I** and **II** have been characterised by EPR spectroscopy and are reminiscent of the presence of a radical species. The emission properties of the parent compound $[Ru(bpy)_2(PhenImHPh)]^{2+}$ were studied as a function of pH and both the lifetimes and intensities decreased upon deprotonation. Photophysical properties, investigated in the absence and presence of an electron acceptor (methylviologen), were distinctly different for the three compounds. Transient absorption features indicate that unique excited states are involved. Theoretical data obtained from DFT calculations in water on the three protonic forms are presented and discussed in the light of the experimental results.

Keywords: density functional calculations · imidazole · photophysical studies · protonic states · ruthenium

Introduction

Even after decades of intensive investigations, ruthenium(II)–polypyridine-type complexes (with $[Ru(bpy)_3]^{2+}$ as the prototype complex) are still opening new avenues in modern coordination chemistry and photochemistry. Indeed, the realms of this coordination metal complex core stem from its high chemical stability and its exceptional photophysical properties.[1,2] Domains extending from electron- and energy-transfer processes to molecular switches, are all based on the well known metal-to-ligand charge transfer (MLCT) transitions within this family of complexes.[3–8] A most important electronic feature of $[Ru(bpy)_3]^{2+}$ is that the lowest excited states are of metal-to-ligand charge transfer character. Upon irradiation in this absorption band, a long-lived excited state ($\approx$600 ns) is reached where the electronic distribution is best described as the presence of a Ru^{III} ion and one electron on the bpy ligands.[9–11] The fact that this state can be quenched through a bimolecular pathway, either by an electron acceptor to generate the highly oxidising Ru^{III} species or by an electron donor to give the formal reducing Ru^{I} form has prompted the use of $[Ru(bpy)_3]^{2+}$ complex as the promising candidate in the field of photoinduced electron transfer studies.[12–15] More sophisticated systems have been developed where this photoactive module was covalently linked to an electron acceptor or donor.

[a] Dr. A. Quaranta, C. Herrero, Dr. W. Leibl, Prof. Dr. A. Aukauloo
iBiTec-S, CEA Saclay, Bât. 532
91191 Gif-sur-Yvette Cedex (France)
E-mail: winfried.leibl@cea.fr
aukauloo@icmo.u-psud.fr

[b] F. Lachaud, Dr. R. Guillot, Dr. M.-F. Charlot, Prof. Dr. A. Aukauloo
Laboratoire de Chimie Inorganique
Institut de Chimie Moléculaire et des Matériaux
d'Orsay UMR CNRS 8182, Univ Paris-Sud
91405 Orsay Cedex (France)
E-mail: mcharlot@icmo.u-psud.fr

Supporting information for this article is available on the WWW under http://www.chemeurj.org/ or from the author.

These diads were elaborated to duplicate the early events in the conversion of light into chemical energy in the reaction centre of photosynthetic systems.[16] In doing so, chemists have overcome the diffusion limits between the donor and acceptor partners and have also gained a better control on the directionality of electron transfer from the donor to the acceptor side. Continuous research is devoted to fine tune both the intramolecular distance between the integrated modules and the nature of the organic spacer, which are crucial parameters for the control of electron transfer rates and understanding the pathways of the electron flow.

Our laboratory is involved in the development of molecular assemblies composed of a photoactive chromophore and a metal complex, the latter being capable of storing oxidative or reductive equivalents. En route towards these target systems, we have prepared and characterised different heteroditopic ligands.[17,18] Recently, we have reported on the synthesis of an imidazole–phenol containing ligand covalently linked to the $[Ru(bpy)_3]^{2+}$ chromophore as a biomimetic model of the His190/TyrZ pair of amino acid residues, which are involved in the catalytic cycle of light-driven water oxidation in photosystem II.[19] A photoinduced electron transfer to an external acceptor (MV^{2+}) was observed to generate the phenoxyl radical concomitantly to the reduction of the photogenerated Ru^{III}. Under identical experimental conditions, a rapid intramolecular reduction of the photogenerated Ru^{III} was evidenced for a related compound lacking the phenol function. It was suspected that in this case the imidazole ring fused to the phenanthroline was the electron donor site. As the imidazole ring is the connecting fragment in this organised assembly of components, we have been interested in elucidating the primary electrochemical and photophysical behaviour of the $[Ru(bpy)_2(PhenImHPh)]^{2+}$ (**II**) complex which contains only the lumophore and the spacer 2-[(3′,5′-di-*tert*-butylbenzene)]imidazo[4,5-*f*][1,10]-phenanthroline (PhenImHPh). Such a family of ligands has been used in the studies on the interaction between transition-metal complexes and DNA.[20–22]

In order to shed light on the influence of the protonic states of the imidazole ring on both the ground and excited states properties of the chromophore/spacer system, we have also isolated and characterised $[Ru(bpy)_2(PhenImPh)]^{+}$ (**I**) and $[Ru(bpy)_2(PhenImH_2Ph)]^{3+}$ (**III**); in the first compound, the secondary amino group is in the deprotonated state, while in the second the imino nitrogen of the imidazole ring is protonated (see below).

The parent compound $[Ru(bpy)_2(PhenImHPh)]^{2+}$ (**II**) and the corresponding deprotonated derivative, **I** and protonated form **III**, have been also characterised by X-ray diffraction technique. The photophysical properties for the three different protonic states were investigated in aqueous solutions at different pH and revealed distinct effects on functional properties of the ensemble. To rationalise the experimental results we will compare them with the theoretical data from DFT calculations obtained on the three water solvated protonic forms of $[Ru(bpy)_2(PhenImHPh)]^{2+}$.

Experimental and Theoretical Results

Synthesis: The ligand PhenImHPh was prepared following a well established imidazole synthetic procedure.[23] An equimolar mixture of phenanthrolinedione and 3,5-di-*tert*-butylbenzaldehyde were heated under reflux in glacial acetic acid containing an excess of ammonium acetate. The compound precipitated as a yellow powder upon cooling. Metathesis of the chloride ions from the $Ru(bpy)_2Cl_2$ source to nitrate ions was realised prior to metallation of the phenanthroline end of the ligand. A methanolic solution of the Ru^{II} salt was heated to reflux in the presence of the ligand. The target compound $[Ru(bpy)_2(PhenImHPh)](PF_6)_2$ was isolated upon addition of an excess of $NaPF_6$ in a concentrated solution of the reacting mixture and was purified by column chromatography on neutral alumina. The protonated form $[Ru(bpy)_2(PhenImH_2Ph)](PF_6)_3$ could be isolated by addition of a dilute solution of HNO_3 followed by an excess of $NaPF_6$ salt. The deprotonated form was isolated after treatment with sodium methoxide.

X-ray structures: The crystal structures of the three different protonated forms of the ruthenium complex were obtained. We summarise here the main crystallographic parameters. X-ray data revealed that the parent compound **II** is described with a chemical formula of $[Ru(bpy)_2(PhenImHPh)](NO_3)_2{\cdot}H_2O{\cdot}3\,MeOH$. An ORTEP view of the monomeric $[Ru(bpy)_2(PhenImHPh)]^{2+}$ unit is shown in Figure 1. ORTEP views of the cationic complexes $[Ru(bpy)_2(PhenImPh)]^{+}$ and $[Ru(bpy)_2(PhenImH_2Ph)]^{2+}$ are reported in the Supporting Information.

A selection of the bond lengths and angles for the units $[Ru(bpy)_2(PhenImPh)]^{+}$, $[Ru(bpy)_2(PhenImHPh)]^{2+}$ and $[Ru(bpy)_2(PhenImH_2Ph)]^{3+}$ are gathered in Table 1.

In all cases, the coordination sphere around the metal ion can be best described as a trigonally distorted octahedral geometry. The angles around the ruthenium centre deviate significantly from ideal octahedral geometry as a result of the constraints imposed by the five-membered chelate rings. The average Ru–N bond length is 2.058, 2.055 and 2.063 Å for **I**, **II** and **III**, respectively. These values fall within the same range as those found for $[Ru(bpy)_3]^{2+}$ (2.056 Å) and related compounds[24] supporting the fact that the protonic states of the ligand do not influence the coordinating properties of the latter to the ruthenium(II) centre. The torsional angle between the imidazole and the phenyl ring is found to be around 17 and 14° for **I** and **II**, respectively while it is 38.5° for **III**. The larger value, when compared with **I** and **II**, can be attributed to the steric hindrance between the protons on the nitrogen atoms of the imidazole and those on the phenyl rings. In the X-ray analysis of **III**, two types of water molecules of crystallisation are identified. Four molecules of water are not involved in the close interaction with either the cation or the anion. While three molecules of water are intercalated between the NH group of the imidazolium ring of two contiguous monomeric units leading to the existence of a hydrogen-bonding network between the

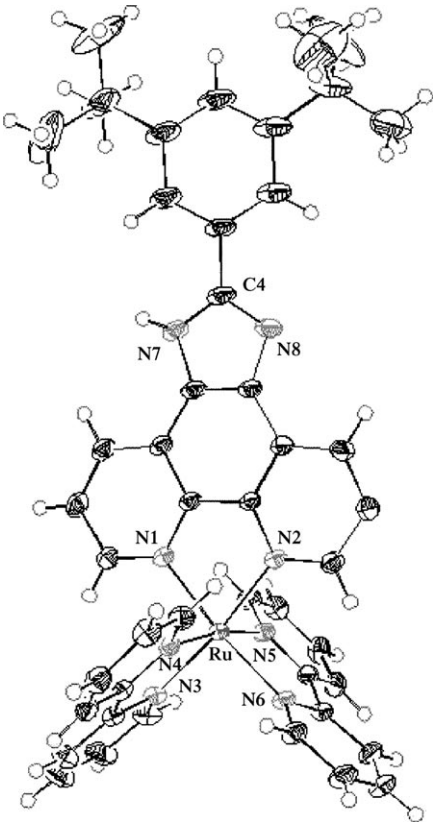

Figure 1. ORTEP drawing of $[Ru(bpy)_2(PhenImHPh)](NO_3)_2{\cdot}H_2O{\cdot}3MeOH$ with partial atom numbering.

Table 1. Selected bond lengths [Å] and angles [°] for complexes $[Ru(bpy)_2(PhenImPh)](PF_6){\cdot}H_2O{\cdot}6MeOH$ (**I**), $[Ru(bpy)_2(PhenImHPh)](NO_3)_2{\cdot}H_2O{\cdot}3MeOH$ (**II**) and $[Ru(bpy)_2(PhenImH_2Ph)](PF_6)_3{\cdot}5H_2O$ (**III**).

	I	II	III
Ru–N1	2.063	2.059	2.058
Ru–N2	2.063	2.068	2.068
Ru–N3	2.061	2.047	2.053
Ru–N4	2.055	2.054	2.070
Ru–N5	2.055	2.052	2.065
Ru–N6	2.061	2.054	2.064
C4–N7	1.352	1.355	1.351
C4–N8	1.352	1.364	1.338
N1-Ru-N2	80.0(8)	79.6(5)	79.5(2)
N3-Ru-N4	78.9(7)	78.5(5)	78.9(9)
N5-Ru-N6	78.9(7)	78.9(8)	78.1(0)

monomeric cationic species. The availability of hydrogen-bonding sites on each edge of the imidazolium ring (NH group) leads to saturation of hydrogen bonds in one dimension as shown in Figure 2.

The hydrogen bond length d(N-H-O_{w1}) is equal to 2.74(1) Å and is thus in the range of very strong hydrogen bonds.[25] The O_{w1}–O_{w3} and O_{w2} are also involved in hydrogen-bonding interaction with an average separation of 2.77 Å.[26] The N-H-O motifs are almost linear with N-H-O_{w1} and N-H-O_{w2} bond angles between 173 and 178°. However, the kink at the N-O-O angles (N-O_{w1}-O_{w3} and N-O_{w2}-O_{w3} 121.2(5) and 112.6(2)°, respectively) confers a zig–zag configuration to the one dimensional hydrogen-bonding network.

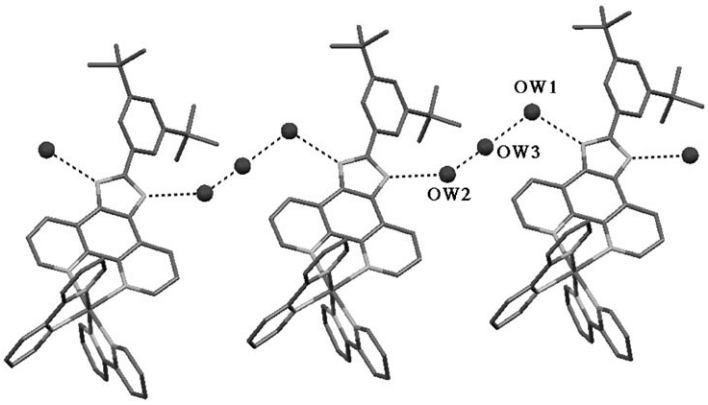

Figure 2. Hydrogen network bonding running between contiguous $[Ru(bpy)_2(PhenImH_2Ph)]$ entities and water molecules.

^{1}H NMR and UV-visible spectra: The protonation and deprotonation steps of the parent complex **II** were monitored by ^{1}H NMR spectroscopy (see Supporting Information). Not surprisingly, upon protonation, a deshielding of the signals for the imidazole containing ligand was observed while an upfield shift of these signals was perceptible upon deprotonation. A small effect was also depicted for the protons in *ortho*-position of the bpy ligands. The major shift (0.2 ppm) was observed for the aromatic proton in *para*-position to the imidazole ring from the deprotonated to the protonated state. This experimental fact suggests that there is no drastic electronic reshuffling upon these chemical processes.

The electronic absorption spectrum of **II** in an organic solvent such as acetonitrile is composed of three sets of bands, one intense band at high energy corresponding to the π–π* transitions of the bpy ligands and a double-humped band in the visible region corresponding to the MLCT transitions in analogy to the spectrum of the $[Ru(bpy)_3]^{2+}$ (Figure 3). However, the spectrum presents unique features like the band at around 340 nm and the shoulder to the MLCT band tailing up to 550 nm which may be attributed to transitions involving the PhenImHPh ligand.

The spectral features for the deprotonated form are similar to those of the parent compound. Nevertheless, we noticed a decrease of intensity of the π–π* transitions at high energy together with an increase in the intensity of the absorption band at 340 nm. It is worthwhile to note that the shoulder to the MLCT band still persists for the deprotonated state. In the case of the protonated state, two main changes are observed on the electronic absorption spectrum in that both bands at 340 nm and the shoulder at 500 nm decrease in intensity. From this experimental data, we can tentatively propose that those bands which fade upon protonation are assigned to the PhenImHPh ligand in the coordination sphere of the ruthenium centre.[27] Notably the absorption spectra are modified in protic solvents like water and

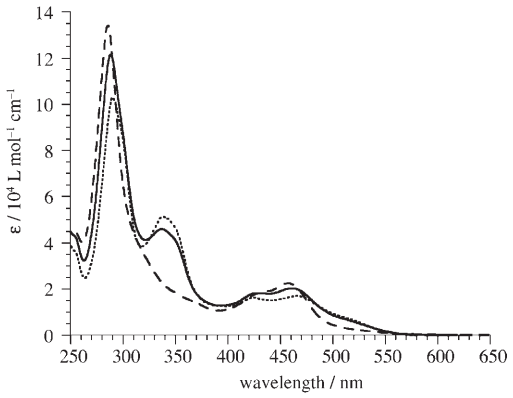

Figure 3. Absorption spectra in CH_3CN for complexes **I** (•••••), **II** (——) and **III** (-----).

methanol (see Supporting Information). The experimental observation is a decrease in intensity of both bands at 340 and 500 nm. This is also the case when methanol is added to a solution of **II** in acetonitrile. Thus it is more likely that the imidazole containing ligand is sensitive to protic solvents, probably due to the formation of hydrogen bonds between the imidazole and the molecules of solvent. Analogous modifications of the ground state absorption spectrum are observed in aqueous solution upon decrease of pH. The pK values of the imidazole ring (pK_1 3.1 ± 0.3, corresponding to deprotonation of the iminium fragment, and pK_2 8.7 ± 0.3, corresponding to deprotonation of the secondary amine) were obtained from titration experiments following the electronic spectral changes (see Supporting Information).

Electrochemistry: Electrochemical studies were performed on the chemically isolated forms of **I**, **II** and **III** in dichloromethane and the data are collected in Table 2.

Table 2. Half-wave potentials for the reduction (^{N}E) and oxidation (^{mi}E) of ligand PhenImHPh and complexes **I**, **II** and **III** in CH_2Cl_2.

Compound	^{II}E[a]	^{I}E[a]	^{i}E[a]	^{ii}E[a]	^{iii}E[a]
PhenImHPh			1.15[b]	1.64[b]	
I	−1.65[b]	−1.35	0.85	1.35[b]	1.43
II	−1.65[b]	−1.35	1.00[b]	1.36[b]	1.46
III	−1.65[b]	−1.35			1.46

[a] Determined by CV at 100 mV s^{-1}; $E=1/2$ ($E_{pa}+E_{pc}$) in V versus SCE in the presence of tetra-*n*-butylammonium perchlorate. [b] Irreversible.

The most surprising observation on the anodic side of the cyclic voltammograms of the three compounds (see Supporting Information) is that the redox potential of the $Ru^{III/II}$ couple is almost unaltered upon remote protonation or deprotonation of the imidazole unit. This result supports the fact that no significant Coulombic effect is exerted on the ruthenium ion by the charge carried on the imidazole ring. Two oxidative processes are observed at lower potentials than that of the $Ru^{III/II}$ redox couple for **I** and **II**. They are assigned to the oxidation of the imidazole–phenyl part of the ligand when compared with the redox behaviour of the ligand only (see Table 2). A shift of about 150 mV to less positive potential is observed for the first anodic wave when going from **II** to **I**, which was logically attributed to the more easy oxidation of the deprotonated imidazole ring. Under our experimental conditions, this wave gains in reversibility in the case of **I**. This observation is most likely due to the loss of the chemical step (proton release) following the one electron-abstraction process in case of compound **II**. An exhaustive one electron electrolysis was performed on **I** and **II** at around 1.0 and 1.2 V versus SCE, respectively. The reversibility of the redox process for compound **I** was justified by the observation of the same cyclic voltammogram trace before and after electrolysis. The X-band EPR spectrum of the frozen sample of the oxidised form of **I** and **II** indicates an isotropic signal centred at $g=2.0024$ in both cases (see Supporting Information) with a peak-to-peak through width of 0.78 mT. No hyperfine coupling is observed not even with the nitrogen atoms of the imidazolate ring.[28] This indicates that the spin density is not centred on the nitrogen atoms and is delocalised on a more extended π-skeleton. On the cathodic side of the cyclic voltammograms of the three complexes no noticeable change is observed at least for the first two reduction waves.

Photochemistry

Emission: The emission spectrum of **II** (between pH ≈3 and ≈9) exhibits a broad band with a maximum at 608 nm and a shoulder at 695 nm (Figure 4). The observed emission

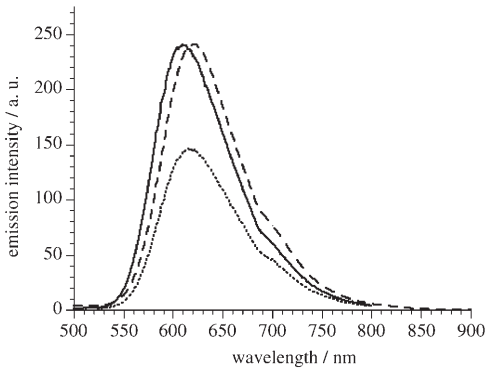

Figure 4. Emission spectra in aqueous solution at pH 2.0 (**III**, -----), 7.6 (**II**, ——) and 10.5 (**I**, •••••) in mixed buffer solutions. Excitation wavelength: 440 nm. Samples optically matched at 440 nm ($A_{440}=0.1$).

lifetime (τ_{em}), ≈800 ns, (see below for more detailed description of each component) is slightly longer than that of $[Ru(bpy)_3]^{2+}$, for which $\tau_{em}=620$ ns. Consistent with the longer lifetime, the emission quantum yield ($\Phi_{em}=0.054$) is higher than that of $[Ru(bpy)_3]^{2+}$ ($\Phi_{em}=0.042$).[29]

The protonation of the imidazole moiety to the protonic state **III** does not alter the emission quantum yield and lifetime, although a red-shift in the emission maximum ($\lambda_{max}=$ 622 nm at pH ≈2) is observed. From the inflection point in

an emission maximum wavelength versus pH plot (see Supporting Information) an apparent pK_1* value of 2.4 ± 0.3 was extracted. However, since a true thermodynamic acid–base equilibrium is not necessarily established within the lifetime of the excited state (<1 μs), the correct pK_1* value for the imidazole protonation in the excited state is calculated using Equation (1)[30] based on the Förster thermodynamic cycle:[31] and references therein

$$pK_1^* = pK_1 + \frac{0.625}{T}(\nu_B - \nu_A) \quad (1)$$

In Equation (1) ν_B and ν_A, the wavenumbers of the 0–0 transition in the base and acid forms, were evaluated as the intersection between the normalised absorption and emission spectra. A pK_1* value of 3.6 was obtained thus indicating that the excited state is a slightly weaker acid than the ground state (pK_1 3.1). Deprotonation of the imidazole to reach the protonic state **I** results in a red shift of the emission accompanied by a decrease in the emission quantum yield ($\Phi_{em}=0.032$) and lifetime (500 ns). The inflection point in the emission maximum wavelength versus pH plot gave an apparent pK_2* 8.9 ± 0.3, while the calculated Förster value is pK_2* 8.3, indicating that the excited state is a slightly weaker base than the ground state (pK_2 8.7).

A closer inspection of the emission kinetic traces obtained upon excitation at 440 nm with ns laser pulses shows a generally biphasic decay containing a minor fast phase whose amplitude relative to the slow phase is virtually independent of pH ($\approx$25%, not shown). The lifetime of this fast phase is $\approx$10 ns (close to time resolution) increasing to 30 ns for **III**. The lifetime of the slow phase decreases from 900 to 500 ns for increasing pH between pH 2 and 11, following a classical titration curve with an apparent pK_2* value of 8.2. The relative yield of the time resolved emission of the protonic state **I** (calculated as the sum of the product of the relative amplitudes and time constants for the different kinetic phases) falls to about 40% of the neutral state. The decrease in the emission yield indicates an apparent pK_2* of 9.0.

Transient absorption: The excited state transient kinetics obtained for the complex in its neutral and protonated forms at pH 7 (**II**) and 2 (**III**), respectively, exhibit a monoexponential decay in the investigated range (400–900 nm) with a lifetime $\tau=(900\pm50)$ ns. At pH 11.0 (**I**), the excited state of the complex in its deprotonated form has a lifetime of (600 ± 50) ns (see inset Figure 5). Those values are in good agreement with the emission lifetimes.

The transient difference absorption spectra taken at 230 ns after excitation for **I**, **II** and **III** (Figure 5) exhibit typical features related to the parent $[Ru(bpy)_3]^{2+}$, that is, a negative band centred at 460 nm due to depletion of the ground state MLCT absorption band, and a very weak transient absorption increase in the region 600–900 nm. For the protonic state **I**, the bleaching in the 400–500 nm region appears to be strongly reduced. However, this decrease in amplitude of the absorption changes at high pH is overestimated to some degree due to changes in sample concentration related to the degassing procedure.[32]

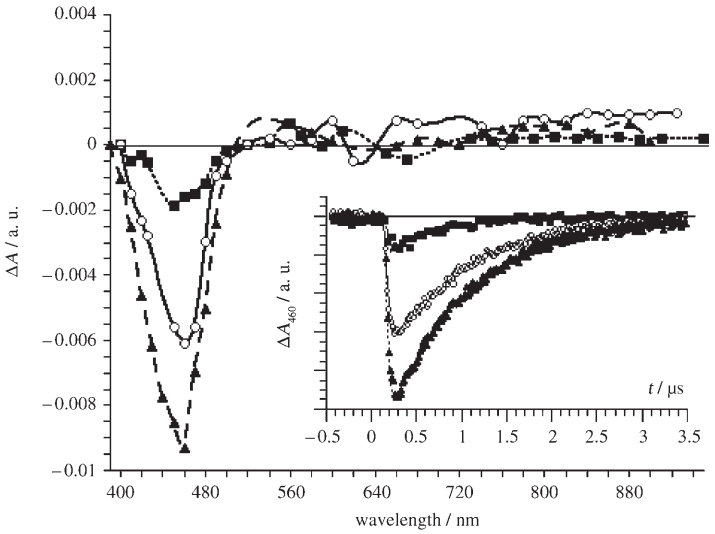

Figure 5. Transient absorption spectra in Argon purged aqueous solutions at pH 2 (10 mM citrate buffer), pH 7 (10 mM HEPES buffer) and pH 11 (10 mM CAPS buffer). Absorption changes taken 230 ns after laser pulse. Excitation wavelength: 440 nm. Samples optically matched at 440 nm ($A_{440}=0.3$); inset: kinetics at 460 nm at pH 2 (**III**, ▲), 7 (**II**, ○) and 11 (**I**, ■).

Photoinduced electron transfer in the presence of an external acceptor: In Figure 6, the kinetic traces of absorption changes at two different wavelengths, 460 and 605 nm are presented. These wavelengths are probes for the recovery of the photogenerated Ru^{III} to Ru^{II} and the presence of $MV^{\bullet+}$ respectively.

At pH 7, the depletion signal at 460 nm exhibits a much shorter lifetime than $MV^{\bullet+}$, indicating that the reduction of Ru^{III} to Ru^{II} is faster than re-oxidation of methyl viologen $MV^{\bullet+}$ to MV^{2+}. This gives evidence that the recovery of Ru^{II} involves a fast intramolecular electron transfer. The low intensity and very fast reappearance of the MLCT band at 460 nm at pH 11, indicates that Ru^{III} is almost not evidenced on this time scale in the deprotonated form of the

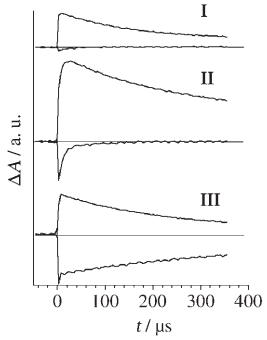

Figure 6. Absorption change kinetics for complexes **I**, **II** and **III** at 460 and 605 nm in Argon purged aqueous solutions in the presence of 10 mM MV^{2+}. Excitation wavelength: 532 nm. Samples optically matched at 532 nm; $A_{532}=0.3$.

imidazole containing ligand. The absorption at 605 nm indicates that methylviologen can still be efficiently reduced. However, the nature of the excited state(s) responsible for the reduction of MV^{2+} remains unclear. To characterise the species after electronic excitation of the Ru^{II} centre, MV^{2+} was replaced by $[Ru(NH_3)_6]^{3+}$, a reversible electron acceptor which is optically transparent in the visible region in both forms. Immediately after irradiation, the transient absorption spectrum collected (see Supporting Information) indicates an absorption band extending from 500 to above 600 nm which can be attributed to the formation of a neutral imidazolyl radical.[33] For **III**, the decay of the kinetic traces at 460 nm and 605 nm is very similar, supporting the fact that the recovery of the photogenerated Ru^{III} to Ru^{II} involves the re-oxidation of $MV^{\bullet+}$ through a bimolecular reaction, thus excluding any intramolecular electron transfer.

These experimental observations will be analysed in more details below in the light of theoretical data.

Theoretical results: We have performed DFT calculations for both the ground and selected excited states (see Charlot et al.[9] and more experimental details in the Experimental Section). As a prerequisite to these calculations the optimised geometric parameters for the ground singlet state S_0, the lowest triplet state T_1 and the lowest D_0 doublet state of the oxidised form were calculated at the (U)B3LYP/LanL2DZ level for the three complexes. They are given in the Supporting Information for states S_0 and T_1 of the three complexes.

DFT calculations realised on isolated molecules (see below) have allowed in many cases to bring conclusive information in rationalising the physical behaviour of coordination metal complexes.[9] However, the extension of these theoretical data from the gas phase to the experimental results in solution is often misleading. For instance, it has been shown that the medium tends to spread the accumulation of charges,[34] so that solvent effects may alter the electronic state of molecules bearing different charges in a dissimilar way. Indeed, electrostatic effects are often much less important for species placed in a solvent with a high dielectric constant than they are in the gas phase.[35] Recent theoretical work on ruthenium–polypyridine complexes have also pointed out the importance of solvent effects to improve the description of electronic spectra.[36–39] Henceforth, owing to the dissymmetry of charges in our molecular systems studied herein, we have analysed our chemical models in solution in the framework of a self-consistent reaction field method (SCRF). The polarizable continuum model (PCM)[40] was used. This approach places the solute in a cavity defined by the union of a series of interlocking atomic spheres within the solvent represented as a polarisable dielectric. All calculations were hence repeated in water. This choice was guided by the fact that all the photophysical experiments were realised in an aqueous solution. Notably the time-consuming geometry optimisations in a water medium was omitted for which convergence problems have been reported.[41] In the aim to clarify the photophysical properties observed for compounds **I**, **II** and **III**, we will focus in this paper on some of our theoretical results obtained for the named compounds in a water surrounding such as i) the relative energies of the different type of molecular orbitals in the ground state, ii) the nature of the low-lying excited singlet states and iii) the nature of the lowest triplet state and the singly oxidised forms. A more in detail analysis of the impact of the surrounding medium will be reported in a forthcoming paper.

Energy levels and molecular orbitals in the ground state: Some typical MOs of **II**, the parent compound for this study, are given in the Supporting Information. A comparison of the ground state MOs of the protonated (**III**) and deprotonated (**I**) complexes with compound **II** allows to establish a correlation between the orbitals of the three complexes (see Supporting Information). The striking evidence is the downshift in energy for all the orbitals located on the ligand upon protonation, that is, a decrease of the electronic density on this part of the molecule. In **I** the negative charge on the imidazole–phenyl fragment is responsible for a HOMO delocalised on L, while the HOMOs of **II** and **III** are d_π orbitals as mostly encountered in such complexes. For the same reason, the LUMO is a combination of the π_1* orbitals of the two bipyridines in **I** and **II** but is the ψ orbital of local *b* symmetry on phenanthroline in **III**.

The mean difference in energy between the set of d_π orbitals and the LUMO is nearly the same that is, 3.41, 3.45 and 3.38 eV for **I**, **II** and **III**, respectively, in comparison to 3.39 eV that we have calculated in the same manner in water for $[Ru(bpy)_3]^{2+}$. The HOMO–LUMO energy gap is 2.84 eV in **I**, 3.36 eV in **II** and 3.28 eV in **III**, the small gap for **I** resulting from the destabilisation of the HOMO on L.

Excited singlet states and electronic absorption spectra: The low-lying singlet excited states of the three complexes in their ground-state geometry were studied using time-dependent DFT (TDDFT) calculations, a method which describes these states in terms of monoexcitations from occupied to vacant MOs of the ground state. Our calculations indicate that for **I**, the lowest excited singlet state S_1 results essentially from a HOMO to LUMO monoexcitation and is hence a ligand-to-bipyridine charge transfer, abbreviated as LBCT. In contrast, S_2 to S_6 states involve either LBCT or charge shifts from the HOMO developed on the imidazole–phenyl part of the ligand to the vacant π orbitals of the phenanthroline moiety of the same ligand, that is, intraligand charge transfers (ILCT). In the case of **I**, MLCT states are encountered at higher energies. For **II**, S_1 results essentially from a charge transfer from d_π to π_1*(bpy) (referred to as MBCT) while for **III** S_1 is obtained by an excitation from the highest d_π MO toward ψ(phen) (MPCT).

Lowest triplet state and oxidised complexes: The lowest triplet state T_1 of each compound was investigated using spin-unrestricted UB3LYP/LanL2DZ calculations followed by geometry optimisation in vacuo. Single point calculations

using this geometry were then performed with the PCM model and water as medium. The same procedure was followed for the ground doublet state D_0 of the oxidised complexes. The theoretical outcomes are reflected by the spin density distributions and are reported in Figure 7 for the T_1 and D_0 states of the three complexes.

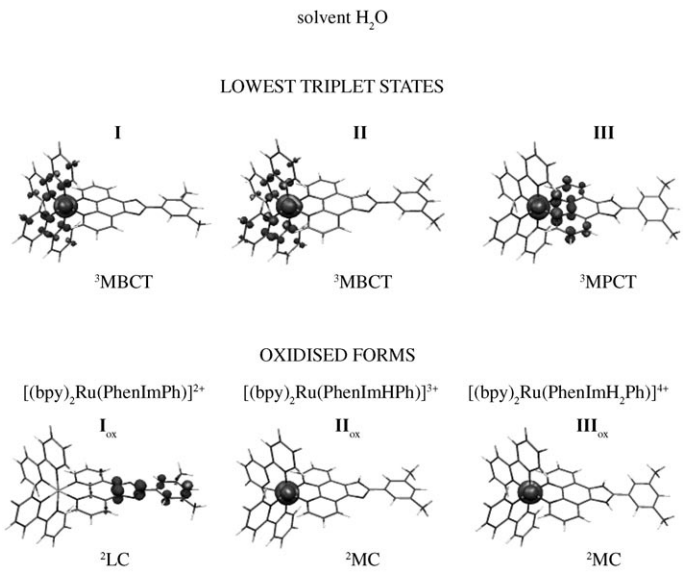

Figure 7. Spin density distribution for the lowest triplet state and the oxidised form of the three complexes calculated in water.

As depicted in Figure 7, all the T_1 states can be viewed as the distribution of one spin on the ruthenium while the other is spread over the two coordinated bipyridines in cases **I** and **II** or over the phenanthroline part of the ligand for **III**. These calculated triplet states resemble that of ruthenium–tris(bipyridine),[9] and can be qualified as the "charge-separated states" in which ruthenium is oxidised in Ru^{III} with partial reduction of the corresponding ligand(s). It is noteworthy that the protonic states of the ligand confer a directionality to the charge separated state: in **I** and **II** the T_1 state is directed from the metal to the bipy motifs (^{3}MBCT), while in **III** it is directed from the metal to the phenanthroline part of the protonated ligand (^{3}MPCT).

Our computed data for the monooxidised form of complex **I** show that almost one spin is localised essentially on the imidazole–phenyl moiety of the ligand and that ruthenium bears no spin (Figure 7). This supports the fact that the first electron abstraction has occurred on the deprotonated imidazole–phenyl part of the ligand (^{2}LC state) and not on the metallic ion which remains formally Ru^{II}. In contrast, for the singly oxidised complexes **II** and **III**, ruthenium bears one spin and oxidation is metal-centred (^{2}MC) as shown in Figure 7.

Discussion

The photophysical behaviour of compounds **I**, **II** and **III** after a flash excitation at 450 nm in the MLCT band show in all cases an emission band centred at around 610 nm. Our calculated lowest triplet states for all three compounds indeed show that they can be described as the charge separated state found for the prototype ruthenium tris(bipyridine) complex. The ruthenium ion is formally in a +III oxidation state characterised by the absence of MLCT transitions and absorption in the 400–460 nm region which is much weaker than the absorption of the ground state. Consequently, a bleaching is observed around 460 nm in the transient spectra (see Figure 5). As Ru^{III} possesses a local unpaired spin, spin-orbit coupling may produce a radiative luminescent decay from the lowest ^{3}MLCT state as observed in Figure 4 for the three complexes. However, other deactivation paths may be efficient or changes of protonation may occur.

On the basis of both experimental and theoretical results, we now propose different schematic pathways for the interpretation of the photoinduced electron transfer studies for compounds **I**, **II** and **III** in the presence of an external electron acceptor. The map for the different electronic and protonic states for compound **I** is shown in Scheme 1.

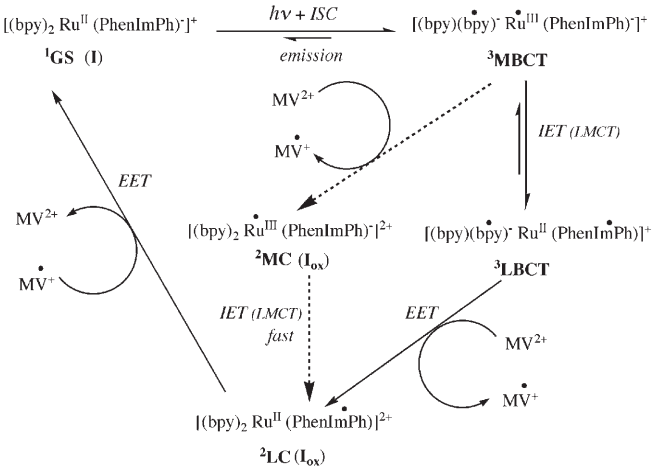

Scheme 1. *hν*: Laser excitation at $\lambda = 440$ nm; ISC: intersystem crossing (^{1}MLCT→^{3}MLCT); EET: external (bimolecular) electron transfer (redox reaction); IET: internal electron transfer.

After irradiation in absence of an external electron acceptor (*hν* step), the emitting ^{3}MBCT is reached. However, in the case of **I**, both the emission intensity at 610 nm (Figure 4) and the bleaching of the MLCT band at 450 nm are less pronounced (Figure 5) as compared to **II** and **III**. These experimental facts suggest the rapid recovery of a Ru^{II} centre. In effect, the oxidising power of the photogenerated Ru^{III} is sufficient to abstract one electron from the deprotonated imidazole part leading to a ^{3}LBCT state through a ligand-to-metal electron transfer. This redox reaction is thermodynamically favourable as confirmed by electrochemical studies. An equilibrium between ^{3}MBCT and ^{3}LBCT may be present in the medium.[42]

In the presence of MV^{2+}, electron density is removed from the high-lying π*(bpy) orbitals occupied in the ^{3}MBCT

state (EET) generating a ^{2}MC state of the oxidised complex (I_{ox}). Simultaneously equilibrium between the low lying triplets is shifted toward ^{3}LBCT. Therefore, these processes can account for the weak absorption changes (Figure 6) in contrast with the formation of a genuine Ru^{III} intermediate. After bimolecular charge shifts reaction between $[(bpy)(bpy^{\bullet})–Ru^{II}(PhenImPh^{\bullet})]^{+}$ and methylviologen, a ^{2}LC state in which the unpaired electron is localised on the deprotonated imidazole–phenyl is reached. An alternate pathway to this state is obtained following an intramolecular electron-transfer process from the deprotonated anionic form of the ligand to photogenerated ruthenium(III) centre, the ^{2}MC state. The X-band EPR data for the monooxidised species of **I** (see Supporting Information) confirm the nature of this oxidised state which is furthermore supported by DFT calculations.

The photoinduced electron pathways for compound **II** (i.e., at pH≈7) is given in Scheme 2.

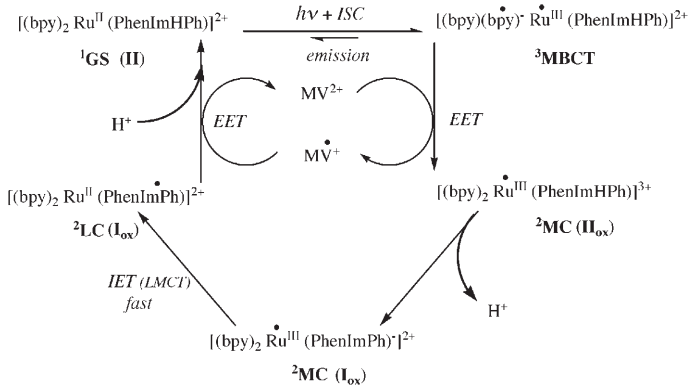

Scheme 2.

The lowest triplet ^{3}MBCT state is reached after light excitation. This state is responsible for the excited state luminescence (Figure 4) and the bleaching at 450 nm observed on the transient spectrum (Figure 5) at neutral pH in absence of an electron acceptor. In the presence of an electron acceptor (MV^{2+}), an electron is transferred from the bipyridines and the bleaching at 460 nm (Figure 6) evidences the formation of Ru^{III} intermediate in agreement with the calculated ground ^{2}MC state of the oxidised complex ($\mathbf{II}_{ox}$). This high valent metal Ru^{III} species ($[(bpy)_2Ru(PhenImHPh)]^{3+}$ on Scheme 2) must be highly polarising therefore enhancing the acidity of the imidazole ring. A subsequent deprotonation step in experimental pH conditions (pH≈7) leads to the oxidised I_{ox} complex $[(bpy)_2Ru(PhenImPh)]^{2+}$. As discussed above, the ground state of I_{ox} is a ^{2}LC state resulting from an internal electron transfer from the deprotonated imidazole fragment of the ligand to Ru^{III}. This proton coupled electron transfer process is most likely at the origin for the rapid recovery of the Ru^{II} MLCT absorption band (Figure 6). An imidazolyl-type radical was evidenced both by EPR spectroscopy and by transient absorption spectroscopy of **II** in the presence of a non-absorbing electron acceptor, $[Ru(NH_3)_6]^{3+}$ (see Supporting Information).

A stepwise proposal for the photodriven charge shifts of compound **III** (pH≈1) is given in Scheme 3.

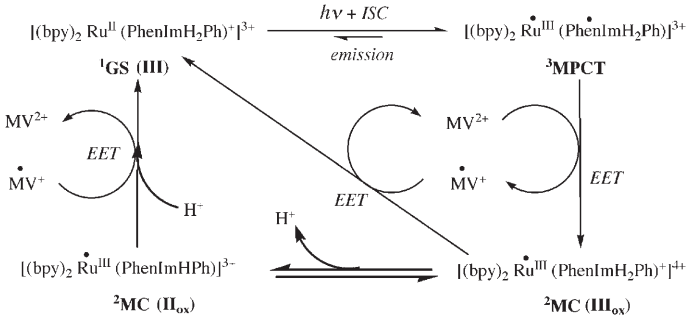

Scheme 3.

The computed lowest triplet state of the protonated complex is a ^{3}MPCT state and the emission properties of **III** are comparable to those of $[Ru(bpy)_3]^{2+}$. Upon irradiation in the presence of an electron acceptor, the charge accumulated on the phenanthroline moiety is transferred to the exogenous MV^{2+}. Both the formation of the $MV^{\bullet+}$ and the bleaching of the MLCT band account for this reaction (Figure 6). The concomitant regeneration of the Ru^{II} and MV^{2+} in this case (Figure 6) indicates that the Ru^{III} is not quenched through an intramolecular electron transfer. This is supported from the electrochemical data where no redox process is depicted before the $Ru^{III/II}$ couple in acidic medium. As can be noticed, the ^{2}MC state is described with a Ru^{III} containing centre and we propose here that a mono deprotonation of the imidazolium may occur under our experimental conditions. However, both oxidised ^{2}MC states (of $\mathbf{III}_{ox}$ or $\mathbf{II}_{ox}$) will experience a similar back electron transfer with $MV^{\bullet+}$ to return to the ground state, as demonstrated by the similar absorption change kinetics at 460 and 605 nm.

Conclusion

In this work, we have described the physical properties of a ruthenium–polypyridine-type complex holding a modified phenanthroline ligand fused with an imidazole ring. The combined electrochemical and photophysical studies supported by DFT calculations have allowed us to understand the electronic perturbations undergoing upon (de)protonation of the imidazole ring. We have shown how the protonic states of the imidazole ring modified drastically the photophysical properties and therefrom the pathways involved in the photoinduced electron transfer process. These results set the basis for future work on more elaborate systems using this chromophore/spacer as the molecular lynchpin to hold a putative metal complex catalyst.

Experimental Section

X-ray crystallography: X-ray diffraction data for $[Ru(bpy)_2(PhenImPh)](PF_6)\cdot H_2O\cdot 6\,MeOH$, $[Ru(bpy)_2(PhenImHPh)](NO_3)_2\cdot H_2O\cdot 3\,MeOH$ and $[Ru(bpy)_2(PhenImH_2Ph)](PF_6)_3\cdot 5\,H_2O$ were collected by using a Kappa X8 APPEX II Bruker diffractometer with graphite-monochromated $Mo_{K\alpha}$ radiation ($\lambda = 0.71073$ Å). The temperature of the crystal was maintained at the selected value (100 K) by means of a 700 series Cryostream cooling device to within an accuracy of ± 1 K. The data were corrected for Lorentz, polarization, and absorption effects. The structures were solved by direct methods using SHELXS-97[43] and refined against F^2 by full-matrix least-squares techniques using SHELXL-97[44] with anisotropic displacement parameters for all non-hydrogen atoms. Hydrogen atoms were located on a difference Fourier map and introduced into the calculations as a riding model with isotropic thermal parameters. All calculations were performed by using the Crystal Structure crystallographic software package WINGX.[45]

One NO_3^- anion of structure $[Ru(bpy)_2(PhenImHPh)](NO_3)_2\cdot H_2O\cdot 3\,MeOH$ appeared to be disordered. The occupancy factors were fixed in the ratio 50:50 for the N atom and one O atom, the two other O atoms being refined with an occupancy factor of 1.0. For this structure also, the hydrogen atom carried by nitrogen is disordered on the two sites with an occupancy rate of 0.5.

The crystal data collection and refinement parameters are given in Table S1 of the Supporting Information.

CCDC-609989, -609990, and -652213 contain the supplementary crystallographic data for this paper. These data can be obtained free of charge from The Cambridge Crystallographic Data Centre via www.ccdc.cam.ac.uk/data_request/cif.

Electrochemical measurements: The experiments were performed with an EGG PAR (model 273 A) electrochemical workstation. The solvents were distilled under nitrogen in the presence of dry calcium chloride and the solution (1 mmol L^{-1} for complexes and ligand and 0.1 mol L^{-1} of tetrabutylammonium perchlorate ($TBAClO_4$) introduced within an argon purged heart shaped cell. Cyclic voltammetry was performed using a glassy carbon electrode (3 mm in diameter) as working electrode, a platinum grid as the counter electrode and an $Ag/AgClO_4$ (0.01 M) electrode in acetonitrile as the reference ($E_{ref} = 0.3$ V/ECS). Electrolyses were carried out at controlled potentials in a three-electrode cell, using a platinum gauze as working electrode, a platinum grid as counter electrode and an $Ag/AgClO_4$ (0.01 M) in acetonitrile electrode as the reference. Low temperature electrolyses were run with 0.2 M of $TBAClO_4$.

UV-visible-NIR spectra: The spectra were recorded with a Varian Cary 5E spectrophotometer (200–1500 nm), with 1 cm quartz cells. Spectroelectrochemical data were obtained by combination of a three electrode thin cell (0.5 mm) mounted in a UV-visible-NIR spectrophotometer. IR spectra were performed with a Perkin–Elmer spectrum 1000 spectrometer, using KBr matrix pellets. NMR spectra were obtained with a Bruker spectrometer AV 360 (360 MHz). The solvents used were $CDCl_3$ or $[D_6]$DMSO. The ^{1}H NMR spectra are given in the Supporting information. EPR spectra were recorded on a X-band spectrometer Elexsys E500 (Bruker) at 100 K. Elemental analyses were performed at Services de Microanalyse, ICSN-CNRS, Gif-sur-Yvette. Mass spectra were recorded on a Finnigan Mat, Mat95S in a BE configuration at low resolution.

Photochemistry: In order to cover a large range of pH and to exclude effects of the buffer, several buffers were used (CAPS, TRIS, HEPES, MES, citrate) as well as their mixture. Steady-state emission spectra were recorded on a Varian Cary Eclipse Spectrofluorimeter upon excitation at 440 nm. All the solutions were optically matched with absorbances of 0.1 at excitation wavelength. Flash-absorption and emission transients were measured with setups of local design. All measurements were done at 296 K. For absorption transients the measuring light was provided by a 450 W xenon lamp. The wavelength was selected with a monochromator (Czerny-Turner) placed after the 10×10 mm, sealed cuvette containing the sample. The sample was excited at 90° to the measuring beam by a flash from a frequency-tripled Nd/YAG laser (Surelight, Continuum) equipped with an OPO. Excitation was set at 440 nm (duration 5 ns, ≈ 5 mJ cm^{-2}). Absorbance changes were detected with a silicon photodiode and signals were amplified by a wideband preamplifier (model 5185, EG&G) before recording by a digital oscilloscope (TDS 3034B, Tektronix). Solutions were purged with Argon for ≈ 20 minutes prior to measurements. A flow-through system was employed to avoid sample degradation due to prolonged exposure to light. For emission transients excitation was done by a flash from a frequency-doubled picosecond Nd/YAG laser (532 nm, duration 25 ps, ≈ 300 μJ cm^{-2}; continuum) or from a frequency-doubled nanosecond Nd/YAG laser (532 nm, duration 7 ns, 2 mJ/cm^2; Quantel). The detection wavelength was selected by interference filters and signals detected with a microchannel plate photomultiplier tube (R2566U, Hamamatsu) and a 7 GHz digitising oscilloscope (IN7000, Intertechnique) or by a digital oscilloscope (TDS 744 A, Tektronix).

Computation methods: Density Functional Theory calculations were carried out using Becke's three-parameter hybrid functional B3LYP[46,47] along with the valence double-ζ basis set LanL2DZ[48,49] including the Los Alamos effective core potential for heavy atoms. All the calculations were performed using the Gaussian 98[50] and Gaussian 03[51] software packages. For consistency reasons we used calculated geometries which were fully optimised in the ground state (closed-shell singlet S_0) for the three compounds. However, in order to decrease the computation time, the two *t*Bu groups on the phenyl ring, which present numerous degrees of freedom without influence on our problem, were replaced by two methyl groups. Starting from the closed-shell S_0 state, time-dependent density functional calculations (TDDFT)[52] were performed to determine the energies and character of the lowest excited singlets and triplets states *in the ground-state geometry*. As photophysical experiments, in absence as well as in the presence of an electron acceptor, may involve the lowest triplet state T_1 and the ground doublet state D_0 of the oxidised complex, these two states were completely studied using a different approach : spin-unrestricted calculations were performed and the corresponding geometries of T_1 and D_0 were fully optimised at the UB3LYP/LanL2DZ level, except for the oxidised form of **III**, a highly-charged (+4) complex for which convergence of the geometry optimisation was not achieved. We have checked that in the open-shell calculations the spin contamination from states of higher spin multiplicity is low by looking at the values of $<S^2>$ (typically 2.006 to 2.009 for a triplet state). The nature of these states was precised by analysis of the corresponding spin-orbitals and spin density distributions, as done by other authors, for instance ref. [53].

In a first step, all these calculations were performed on the isolated molecule (gas phase) and, in a second step, solvent effects were modelled in the framework of a self-consistent reaction field method (SCRF). Calculations on the gas-phase optimised geometries were performed with the polarized dielectric model (PCM)[40,54] using the integral equation formalism (IEF).[55,56] The selected solvent was water and all parameters were kept to their implemented Gaussian 03 values. No geometry optimisation was attempted in the solvent.

Materials: Ruthenium trichloride was purchased from the Aldrich Chemical Company. 2,2′-Bipyridine (bpy) and 1,10-phenanthroline (phen) were obtained from Janssen Chemical Company. 1,10-Phenanthroline-5,6-dione,[57] 3,5-di-*tert*-butylbenzaldehyde,[58] and $[Ru(bpy)_2Cl_2]$[59] were synthesised as described in the literature.

PhenImHPh: A 1:1 mixture of 5,6-phenanthrolinedione (420 mg, 2 mmol) and 3,5-di-*tert*-butyl-benzaldehyde (444 mg, 2 mmol) in AcOH together with an excess of NH_4OAc (3.1 g, 40 mmol) was heated to reflux. A yellow solid precipitates out upon cooling, which was isolated by filtration and washed with water and vacuum dried (610 mg, ≈75%). ^{1}H NMR ($[D_6]$DMSO, 360 MHz): δ = 13.70 (s, NH), 9.05 (d, 2H), 8.90 (d, 2H), 8.20 (d, 2H) 7.86 (m, 2H), 7.60 (s, 1H), 1.50 ppm (s, 18H); IR: $\tilde{\nu}$ = 3385 (NH), 2952, 2900, 2864 (CH), 1643 cm^{-1} (C=N Phen); ESI MS: *m*/*z* (%): 409.2 $[M+H]^+$.

Complex II: $[Ru(bpy)_2Cl_2]$ (242 mg, 0.5 mmol) was treated with $AgNO_3$ (170 mg, 1.0 mmol) in MeOH (5 mL) for 1 h. The AgCl precipitate was filtered off and the filtrate evaporated to dryness. Ligand PhenImHPh (204 mg, 0.5 mmol) was added to the ruthenium salt in MeOH (10 mL) and stirred under reflux for 3 h. The solvent was removed by rotary evap-

oration and the crude product was purified by column chromatography on neutral alumina (CH_2Cl_2/MeOH 90:10) to afford **II**$(NO_3)_2$ (353 mg, 72%) as an orange solid. The corresponding hexaflurophosphate salt was isolated upon addition of a saturated aqueous solution of $NaPF_6$ to a concentrated solution of **II**$(NO_3)_2$ in methanol. ^{1}H NMR ([D$_6$]DMSO, 360 MHz): δ = 9.05 (d, 2H), 8.90, 8.85 (d, 4H), 8.27 (d, 2H), 8.22 (t, 2H), 8.10 (t, 2H), 7.89 (d, 2H), 7.81 (d, 2H), 7.73 (dd, 2H), 7.59 (m, 4H), 7.39 (m, 3H), 1.38 ppm (s, 18H); IR: $\tilde{\nu}$ = 2951, 2902, 2863 (CH), 1623 (C=N), 1360 cm^{-1} (N=O, NO_3^-); UV λ_{max} (ε) = 240 (26500), 250 (sh, 22000), 287 (61500), 335 (23400), 430 (9500), 460 (10000), 520 nm (sh, 3000); ESI MS: *m*/*z* (%): 411.3 (100) $[M]^{2+}$; elemental analysis calcd (%) for $C_{47}H_{44}N_{10}O_6Ru\cdot 2H_2O$ (982.02): C 57.48, H 4.93, N 14.26; found: C 57.90, H 5.09, N 14.20.

Complex III: **II**$(NO_3)_2$ (67 mg, 0.07 mmol) was dissolved in methanol (3 mL). To this solution was added 1 M nitric acid (80 μL). This solution was stirred for an hour, and then concentrated under reduced pressure. The hexafluorophosphate salt was isolated upon addition of a saturated aqueous solution of $NaPF_6$ to give an orange powder (78 mg, 85%). ^{1}H NMR ([D$_6$]DMSO, 360 MHz): δ = 9.13 (d, 2H), 8.90, 8.86 (d, 4H), 8.23 (t, 2H), 8.18 (d, 2H), 8.13 (t, 2H), 8.03 (d, 2H), 7.9 (m, 4H), 7.6 (m, 5H), 7.37 (t, 2H), 1.43 ppm (s, 18H); IR: $\tilde{\nu}$ = 3104 (NH), 2952, 2900, 2864 (CH), 1624 cm^{-1} (C=N phen); UV: λ_{max} (ε) = 286 (67000), 430 (10000), 460 nm (11500); ESI MS: *m*/*z* (%): 411.2 (100) $[M]^{2+}$; elemental analysis calcd (%) for $C_{47}H_{45}F_{18}N_8P_3Ru\cdot 3H_2O$ (1311.92): C 43.03, H 3.92, N 8.54; found C 43.17, H 4.09, N 8.62.

Complex I: **II**$(NO_3)_2$ (67 mg, 0.07 mmol) was dissolved in acetonitrile (3 mL). An excess of sodium methoxide was added to this solution. The mixture was stirred for 2 h then filtered to remove undissolved material. The filtrate evaporated to dryness. The solid was dissolved in a small amount of methanol and precipitated with an excess of $NaPF_6$ salt (62 mg, 87%). ^{1}H NMR ([D$_6$]DMSO, 250 MHz): δ = 8.97 (d, 2H), 8.90, 8.86 (d, 4H), 8.27 (d, 2H), 8.22 (t, 2H), 8.16 (t, 2H), 7.89 (d, 2H), 7.71 (m, 4H), 7.60 (m, 4H), 7.36 (m, 3H), 1.40 ppm (s, 18H); IR: $\tilde{\nu}$ = 2954, 2900, 2866 (CH), 1629 cm^{-1} (C=N phen); UV: λ_{max} (ε) = 240 (23500), 250 (sh, 18000), 290 (55000), 337 (26000), 425 (9000), 460 (8000), 520 (sh, 3000); ESI MS: *m*/*z* (%): 411.3 (100) $[M]^{2+}$, 821.3 (21) $[M]^{+}$; elemental analysis calcd (%) for $C_{47}H_{43}F_6N_8PRu\cdot H_2O\cdot CH_3OH$ (1015.99): C 56.74, H 4.86, N 11.03; found C 56.80, H 4.92, N 11.20.

Acknowledgements

This work was supported by the CNRS (ANR Blanc HYPHO) and the European Commission (NEST STREP SOLAR-H contract No 516510). We thank the Centre Informatique National de l'Enseignement Supérieur at Montpellier (France) and the Institut du Développement et des Ressources en Informatique Scientifique at Orsay (France) for providing calculation means. C.H. is grateful to the International Chair of Blaise Pascal for a scholarship.

[1] V. Balzani, A. Juris, *Coord. Chem. Rev.* **2001**, *211*, 97–115.
[2] K. Kalyanasundaram, *Coord. Chem. Rev.* **1982**, *46*, 159–244.
[3] N. D. McClenaghan, Y. Leydet, B. Maubert, M. T. Indelli, S. Campagna, *Coord. Chem. Rev.* **2005**, *249*, 1336–1350.
[4] V. Balzani, A. Credi, M. Venturi, *Coord. Chem. Rev.* **1998**, *171*, 2–16.
[5] P. D. Beer, P. A. Gale, *Angew. Chem.* **2001**, *113*, 502–532; *Angew. Chem. Int. Ed.* **2001**, *40*, 486–516.
[6] S. Welter, K. Brunner, J. W. Hofstraat, L. De Cola, *Nature* **2003**, *421*, 54–58.
[7] B. Schlicke, L. De Cola, P. Belser, V. Balzani, *Coord. Chem. Rev.* **2000**, *208*, 267–275.
[8] R. Passalacqua, F. Loiseau, S. Campagna, Y.-Q. Fang, G. S. Hanan, *Angew. Chem.* **2003**, *115*, 1646–1649; *Angew. Chem. Int. Ed.* **2003**, *42*, 1608–1611.
[9] M.-F. Charlot, Y. Pellegrin, A. Quaranta, W. Leibl, A. Aukauloo, *Chem. Eur. J.* **2006**, *12*, 796–812.
[10] C. Daul, E. J. Baerends, P. Vernooijs, *Inorg. Chem.* **1994**, *33*, 3538–3543.
[11] J. K. McCusker, *Acc. Chem. Res.* **2003**, *36*, 876–887.
[12] C. R. Bock, J. A. Connor, A. R. Gutierrez, T. J. Meyer, D. G. Whitten, B. P. Sullivan, J. K. Nagle, *J. Am. Chem. Soc.* **1979**, *101*, 4815–4824.
[13] M. Kirch, J.-M. Lehn, J. P. Sauvage, *Helv. Chim. Acta* **1979**, *62*, 1345–1384.
[14] N. Kitamura, H.-B. Kim, S. Sumio, S. Tazuke, *J. Phys. Chem.* **1989**, *93*, 5750–5756.
[15] H.-B. Kim, N. Kitamura, Y. Kawanishi, S. Tazuke, *J. Phys. Chem.* **1989**, *93*, 5757–5764.
[16] F. Scandola, C. Choiorboli, M. T. Indelli, M. A. Rampi, *Vol. 3* (Ed.: V. Balzani), Wiley-VCH, Weinheim, **2001**, pp. 337–408.
[17] Y. Pellegrin, K. E. Berg, G. Blondin, E. Anxolabéhère-Mallart, W. Leibl, A. Aukauloo, *Eur. J. Inorg. Chem.* **2003**, 1900–1910.
[18] Y. Pellegrin, A. Quaranta, P. Dorlet, M.-F. Charlot, W. Leibl, A. Aukauloo, *Chem. Eur. J.* **2005**, *11*, 3698–3710.
[19] F. Lachaud, A. Quaranta, Y. Pellegrin, P. Dorlet, M.-F. Charlot, S. Un, W. Leibl, A. Aukauloo, *Angew. Chem.* **2005**, *117*, 1560–1564; *Angew. Chem. Int. Ed.* **2005**, *44*, 1536–1540.
[20] H. Xu, K.-C. Zheng, H. Deng, L.-J. Lin, Q.-L. Zhang, L.-N. Ji, *New J. Chem.* **2003**, *27*, 1255–1263.
[21] Y. Xiong, L.-N. Ji, *Coord. Chem. Rev.* **1999**, *185–186*, 711–733.
[22] L.-N. Ji, X.-H. Zou, J.-G. Liu, *Coord. Chem. Rev.* **2001**, *216–217*, 513–536.
[23] E. A. Steck, A. R. Day, *J. Am. Chem. Soc.* **1943**, *65*, 452–456.
[24] D. P. Rillema, D. S. Jones, C. Woods, H. A. Levy, *Inorg. Chem.* **1992**, *31*, 2935–2938.
[25] G. C. Pimentel, A. L. McClellan, *The hydrogen bond*, W. H. Freeman, San Francisco, **1960**, p. 260.
[26] M. C. Munoz, R. Ruiz, M. Traianidis, A. Aukauloo, J. Cano, Y. Journaux, I. Fernandez, J. R. Pedro, *Angew. Chem.* **1998**, *110*, 1933–1936; *Angew. Chem. Int. Ed.* **1998**, *37*, 1833–1836.
[27] J.-Z. Wu, Y. Guang, S. Chen, L. N. Ji, J.-Y. Zhou, Y. Xu, *Inorg. Chim. Acta* **1998**, *283*, 17–23.
[28] J. Abe, T. Sano, M. Kawano, Y. Ohashi, M. M. Matsushita, T. Iyoda, *Angew. Chem.* **2001**, *113*, 600–602; *Angew. Chem. Int. Ed.* **2001**, *40*, 580–582.
[29] D. M. Roundhill, *Photochemistry and photophysics of metal complexes*, Plenum Press, New York, **1994**, pp. 165–215.
[30] The equation is obtained assuming that the entropy changes accompanying protonation are the same in the ground and in the excited states.
[31] R. J. Crutchley, N. Cress, A. B. P. Lever, *J. Am. Chem. Soc.* **1983**, *105*, 1170–1178.
[32] We noticed a loss of solubility associated to the increase of solvent basicity. During the degassing procedure, especially at high pH, part of the complex adheres on the cuvette walls. The amplitude of signal might thus be affected due to a decreased bulk concentration of the compound. Due to the long measurement times to record the full spectrum, absorption change measurements are much more susceptible to be affected than measurements of emission spectra.
[33] R. H. Riem, A. McLachlan, G. R. Coraor, E. J. Urban, *J. Org. Chem.* **1971**, *36*, 2272–2275.
[34] M. K. Nazeeruddin, Q. Wang, L. Cevey, V. Aranyos, P. Liska, E. Figgemeier, C. Klein, N. Hirata, S. Koops, S. A. Haque, J. R. Durrant, A. Hagfeldt, A. B. P. Lever, M. Grätzel, *Inorg. Chem.* **2006**, *45*, 787–797.
[35] J. B. Foresman, Æ. Frisch in *Exploring chemistry with electronic structure methods*, Gaussian, Inc., Pittsburg, PA, **1996**, p. 237.
[36] J. E. Monat, J. H. Rodriguez, J. K. McCusker, *J. Phys. Chem. A* **2002**, *106*, 7399–7406.
[37] J. F. Guillemoles, V. Barone, L. Joubert, C. Adamo, *J. Phys. Chem. A* **2002**, *106*, 11354–11360.
[38] S. R. Stoyanov, J. M. Villegas, D. P. Rillema, *Inorg. Chem. Commun.* **2004**, *7*, 838–841.

[39] F. De Angelis, S. Fantacci, A. Sgamelotti, F. Cariati, D. Roberto, F. Tessore, R. Ugo, *Dalton Trans.* **2006**, 852–859.
[40] E. Cancès, B. Menucci, J. Tomasi, *J. Chem. Phys.* **1997**, *107*, 3032–3041.
[41] F. De Angelis, S. Fantacci, A. Selloni, *Chem. Phys. Lett.* **2004**, *389*, 204–208.
[42] Indeed, TDDFT calculations in water starting from T_1 (^{3}B symmetry) point out that T_2, lying 0.09 eV above T_1 is the ^{3}MBCT of ^{3}A symmetry corresponding to a promotion of d_π electrons to the second combination of π_1*(bpy) orbitals. T_2 has therefore exactly the same photophysical properties as T_1. In addition, T_3, a ^{3}LBCT state is calculated only 0.04 eV higher in energy.
[43] G. M. Sheldrick, *SHELXS-97*, University of Göttingen, Göttingen (Germany), **1990**.
[44] G. M. Sheldrick, *SHELXL-97*, University of Göttingen, Göttingen (Germany), **1997**.
[45] L. J. Farrugia, *J. Appl. Crystallogr.* **1999**, *32*, 837–838.
[46] A. D. Becke, *J. Chem. Phys.* **1993**, *98*, 5648.
[47] C. Lee, W. Yang, R. G. Parr, *Phys. Rev. B* **1988**, *37*, 785.
[48] T. H. Dunning Jr, P. J. Hay, *Mod. Theor. Chem.* **1976**, p. 1–28.
[49] P. J. Hay, W. R. Wadt, *J. Chem. Phys.* **1985**, *82*, 270–283.
[50] Gaussian 98, Revision A.11.3, M. J. Frisch, G. W. Trucks, H. B. Schlegel, G. E. Scuseria, M. A. Robb, J. R. Cheeseman, V. G. Zakrzewski, J. A. Montgomery, Jr., R. E. Stratmann, J. C. Burant, S. Dapprich, J. M. Millam, A. D. Daniels, K. N. Kudin, M. C. Strain, O. Farkas, J. Tomasi, V. Barone, M. Cossi, R. Cammi, B. Mennucci, C. Pomelli, C. Adamo, S. Clifford, J. W. Ochterski, G. A. Petersson, P. Y. Ayala, Q. Cui, K. Morokuma, P. Salvador, J. J. Dannenberg, D. K. Malick, A. D. Rabuck, K. Raghavachari, J. B. Foresman, J. Cioslowski, J. V. Ortiz, A. G. Baboul, B. B. Stefanov, G. Liu, A. Liashenko, P. Piskorz, I. Komaromi, R. Gomperts, R. L. Martin, D. J. Fox, T. Keith, M. A. Al-Laham, C. Y. Peng, A. Nanayakkara, M. Challacombe, P. M. W. Gill, B. Johnson, W. Chen, M. W. Wong, J. L. Andres, C. Gonzalez, M. Head-Gordon, E. S. Replogle, J. A. Pople, Gaussian, Inc., Pittsburgh PA, **2002**.
[51] Gaussian 03, Revision D.02, M. J. Frisch, G. W. Trucks, H. B. Schlegel, G. E. Scuseria, M. A. Robb, J. R. Cheeseman, J. A. Montgomery, Jr., T. Vreven, K. N. Kudin, J. C. Burant, J. M. Millam, S. S. Iyengar, J. Tomasi, V. Barone, B. Mennucci, M. Cossi, G. Scalmani, N. Rega, G. A. Petersson, H. Nakatsuji, M. Hada, M. Ehara, K. Toyota, R. Fukuda, J. Hasegawa, M. Ishida, T. Nakajima, Y. Honda, O. Kitao, H. Nakai, M. Klene, X. Li, J. E. Knox, H. P. Hratchian, J. B. Cross, V. Bakken, C. Adamo, J. Jaramillo, R. Gomperts, R. E. Stratmann, O. Yazyev, A. J. Austin, R. Cammi, C. Pomelli, J. W. Ochterski, P. Y. Ayala, K. Morokuma, G. A. Voth, P. Salvador, J. J. Dannenberg, V. G. Zakrzewski, S. Dapprich, A. D. Daniels, M. C. Strain, O. Farkas, D. K. Malick, A. D. Rabuck, K. Raghavachari, J. B. Foresman, J. V. Ortiz, Q. Cui, A. G. Baboul, S. Clifford, J. Cioslowski, B. B. Stefanov, G. Liu, A. Liashenko, P. Piskorz, I. Komaromi, R. L. Martin, D. J. Fox, T. Keith, M. A. Al-Laham, C. Y. Peng, A. Nanayakkara, M. Challacombe, P. M. W. Gill, B. Johnson, W. Chen, M. W. Wong, C. Gonzalez, J. A. Pople Gaussian, Inc., Wallingford CT, **2004**.
[52] M. E. Casida, C. Jamorski, K. C. Casida, D. R. Salahub, *J. Chem. Phys.* **1998**, *108*, 4439.
[53] J. M. Villegas, S. R. Stoyanov, W. Huang, L. L. Lockyear, J. H. Reibenspies, D. P. Rillema, *Inorg. Chem.* **2004**, *43*, 6383–6396.
[54] M. Cossi, G. Scalmani, N. Rega, V. Barone, *J. Chem. Phys.* **2002**, *117*, 43–54.
[55] B. Mennucci, J. Tomasi, *J. Chem. Phys.* **1997**, *106*, 5151–5168.
[56] J. Tomasi, B. Mennucci, E. Cancès, *J. Mol. Struct Theochem* **1999**, *464*, 211–226.
[57] W. Paw, R. Eisenberg, *Inorg. Chem.* **1997**, *36*, 2287–2293.
[58] E. Rose, B. Andrioletti, P. P. Ramasamy, *J. Porphyrins Phthalocyanines* **2002**, *6*, 602–606.
[59] B. P. Sullivan, T. J. Meyer, *Inorg. Chem.* **1978**, *17*, 3334–3341.

Received: February 2, 2007
Published online: July 16, 2007

